

pubs.acs.org/Macromolecules Article

Complex Phase Behavior in Binary Blends of AB Diblock Copolymer and ABC Triblock Terpolymer

So Jung Park, Frank S. Bates,* and Kevin D. Dorfman*



Cite This: Macromolecules 2023, 56, 1278-1288



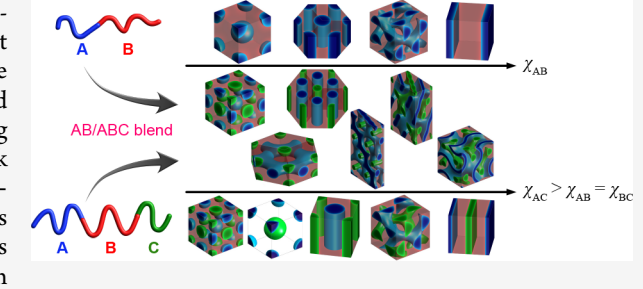
ACCESS I

III Metrics & More

Article Recommendations

Supporting Information

ABSTRACT: Blending block polymers with different block compositions provides an opportunity to create nanostructures that are not accessible from neat block copolymer melts. In this study, we investigate the equilibrium phase behavior in binary blends composed of an AB diblock copolymer and an ABC triblock terpolymer, using self-consistent field theory (SCFT). Blending these simple linear block polymers results in complex phase behaviors, including unusual coreshell network phases with asymmetric core and shell volume fractions and a new cylinder-in-O⁷⁰ hybrid network phase. The phase diagrams with respect to segregation strength and blend composition reveal an



unexpected morphological richness, including 15 ordered phases, illustrating the potential inherent in blending these relatively simple components.

INTRODUCTION

Block polymers exhibit a rich phase behavior where a variety of ordered structures self-assemble on mesoscopic length scales through microphase separation of thermodynamically incompatible constituent blocks. 1,2 Simple AB diblock copolymer melts form lamellar, hexagonally packed cylinder, and bodycentered cubic (bcc) sphere phases below the order-disorder transition temperature, where the ordered-state symmetry depends primarily on the volume fraction f_A of A blocks. Among the various morphologies observed in block polymers, network phases consisting of triply continuous nanochannels are of significant interest due to their potential applications in advanced nanotechnologies such as photonic crystals, solar cells, and membranes.^{3–8} For linear AB diblock copolymer melts, the double gyroid phase (denoted G and having Ia3d (#230) space group symmetry), which contains two separate networks, and the orthorhombic Fddd single network phase (termed O⁷⁰ with Fddd (#70) space group symmetry) have been identified as equilibrium structures within a narrow composition window about 0.02–0.03 wide in f_A . 9–15 Both the G and O⁷⁰ morphologies are characterized by 3-fold units connected together to form the space-filling 3-D network structures. Introducing a third C component onto an AB diblock copolymer expands the parameter space to five independent parameters (two compositional parameters, f_A and $f_{\rm B}$, and three Flory-Huggins interaction parameters, $\chi_{\rm AB}$, $\chi_{\rm BC}$, and $\chi_{\rm AC}$, which define the segregation strength between the blocks). This large parameter space in ABC triblock terpolymers leads to a greater number of ordered phases than with AB diblock copolymers, including two types of gyroid structures: a pentacontinuous core-shell G phase and a triply

continuous alternating GA morphology consisting of two interwoven A and C networks. 16-19

For designing advanced optical materials and nanoporous templates with self-assembled network structures, morphological variety in the network phases is highly desirable. However, in neat AB diblock copolymers or ABC triblock terpolymers, the network phases are stable only within narrow composition windows, which limits the design possibilities. Blending two block copolymers with different block compositions extends the morphological variability, a wellestablished strategy for controlling the ordered morphology by modifying the interfacial curvatures. For example, binary blends have been used to produce new ordered nanostructures, such as Frank-Kasper phases, that are not stable in neat block copolymer melts.²⁰⁻²³ However, most prior studies have focused on binary blends of diblock copolymers or diblock copolymer mixed with homopolymer and are thus limited to two-microdomain phases.^{23–30}

In terms of morphological diversity, an AB/ABC blend system is an attractive candidate for designing new threemicrodomain network structures. Such blends can extend the range of triblock terpolymer network phases by modifying interfacial curvature through incorporation of diblock copolymer chains within 3-domain (A, B, and C) structures. While

Received: October 27, 2022 Revised: December 11, 2022 Published: January 27, 2023





the phase behavior of the AB diblock and ABC triblock components is relatively well understood based on theory 10,11,19 and experiment, 1,2,16,17,31 the phase behavior of binary AB/ABC blends has barely been probed due in part to challenges posed by an expansive parameter space, which includes eight independent parameters (three χ_{ij} , three f_{ij} , the ratio of degrees of polymerization $N_{\rm AB}/N_{\rm ABC}$, and the blend composition). Because each of these parameters influences block polymer self-assembly, the AB/ABC blend is expected to exhibit a rich complement of phases.

While there are a few theoretical studies^{32,33} and experiments^{22,34,35} on AB/ABC blends demonstrating formation of lamellae, core-shell cylinders, and core-shell spheres, where C core microdomains are surrounded by B shells in an A matrix, there are fewer reports 22,34,36 of tricontinuous network forming AB/ABC mixtures. Early work by Abetz and coworkers experimentally investigated AB/ABC blends using a series of polystyrene, polybutadiene, and poly(methyl methacrylate) based block polymers. 22,34 They reported formation of the core-shell double-gyroid morphology from blends of lamellar forming ABC triblock and lamellar forming AB diblock polymers. Another experimental paper, published by Kim and co-workers, ³⁶ described an unusual core—shell double gyroid produced in a binary blend of asymmetric polyisopreneb-polystyrene-b-poly(2-vinylpyridine) (ISP) triblock terpolymer, which forms a hybrid structure of spheres and cylinders with tetragonal packing in the neat melt and an asymmetric bcc forming polyisoprene-b-polystyrene (IS) diblock copolymer. Although rather limited in the extent of the vast parameter space that was explored, these experimental results suggest that blending AB diblock and ABC triblock polymers can stabilize unusual morphologies distinct from those accessible with neat block polymer melts.

Inspired by the potential for new network and other phase formation, we used self-consistent field theory (SCFT) calculations to investigate the phase behavior of binary blends composed of the diblock and triblock polymers illustrated in Figure 1. This illustration highlights the complexity inherent in such mixtures, shown here for an asymmetric diblock (f_A = 0.357) that passes through all four ordered states with increasing segregation strength, in combination with compositionally asymmetric $(f_A > f_C)$ or symmetric $(f_A = f_C)$ triblocks, which exhibit different complements of phases. Even these limited results demonstrate the expansive opportunities for creating new morphologies through blending of two relatively simple polymer molecular architectures. Our SCFT calculations reveal that varying just one parameter, i.e., blend composition, results in unexpected phase behaviors. Additional motivation to more thoroughly explore the consequences of mixing molecular architectures is provided in Figure 2, where an alternating gyroid (GA) forming triblock is blended with a G-forming diblock. Here, we choose G^A-forming ABC block copolymer and G-forming diblock copolymer, inspired by our previous work on the ternary phase diagram of GA-forming AB/BC/ABC blends,³⁷ where the AB/ABC blend system corresponds to one side of the triangular ternary phase diagram. Even with this specific example, a remarkably rich set of hybrid morphologies emerge as the composition is swept from pure triblock to pure diblock, extending the range of network phases.

This article describes the construction of phase diagrams as a function of segregation strength and blend composition for several combinations of AB and ABC block polymers, based on

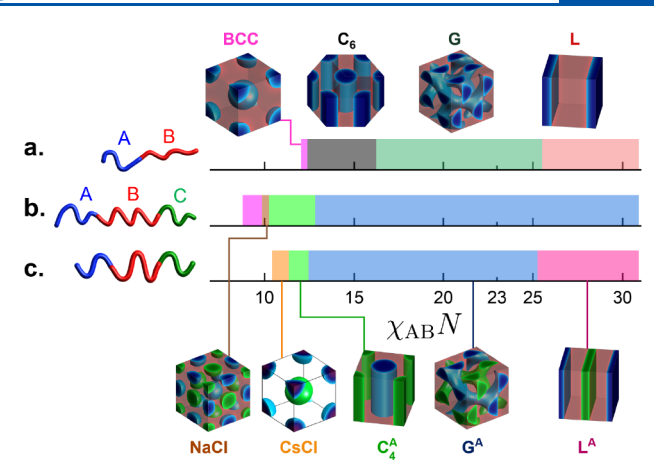


Figure 1. Block polymers adopted in our SCFT calculations: AB diblock copolymer, asymmetric ABC triblock terpolymer, and symmetric ABC triblock terpolymer. (a) Equilibrium phase sequence observed in the AB diblock copolymer of A block volume fraction f_A = 0.357 as a function of $\chi_{AB}N$, where N is the total degree of polymerization of diblock: body-centered cubic sphere, BCC \rightarrow hexagonal-packed cylinders, $C_6 \rightarrow$ double gyroid, $G \rightarrow$ lamellae, L. (b) Equilibrium phase sequence observed in the asymmetric ABC triblock terpolymer, where the block lengths are $N_{\rm A}'=0.47N,\,N_{\rm B}'=0.47N$ 1.5N, and $N_C' = 0.35N$: BCC \rightarrow NaCl-type binary spheres, NaCl \rightarrow square-packed alternating cylinders, $C_4^A \rightarrow$ alternating gyroid, G^A . (c) Equilibrium phase sequence observed in the symmetric ABC triblock terpolymer, where the block lengths are $N'_{A} = 0.36N$, $N'_{B} = 1.08N$, and $N_{\rm C}' = 0.36N$: CsCl-type binary spheres, CsCl \rightarrow C₄^A \rightarrow G^A \rightarrow alternating lamellae, L^A. For both triblock terpolymers, $\chi_{AB} = \chi_{BC}$ and $\chi_{AC} = 1.75 \chi_{AB}$.

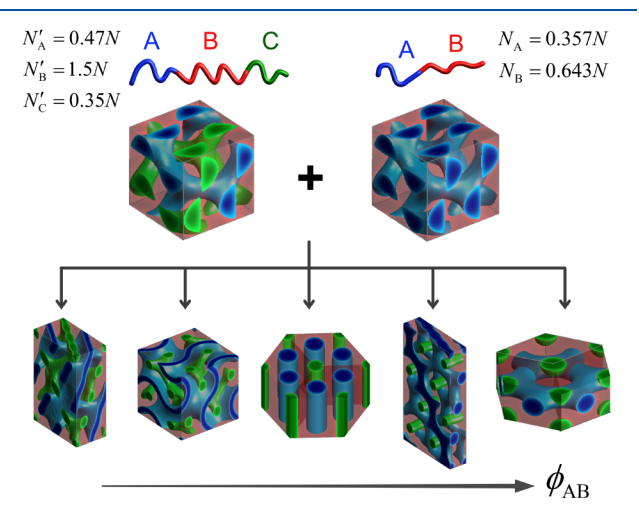


Figure 2. Schematic illustrating blending the G^A -forming, asymmetric ABC triblock terpolymer and the G-forming AB diblock copolymer, which results in complex phase behaviors with the phase sequence core—shell Fddd (CSO⁷⁰) \rightarrow core—shell gyroid (CSG) \rightarrow hexagonal-packed alternating cylinders (C_{6a}^A) \rightarrow cylinder-in-O⁷⁰ (CylO⁷⁰) \rightarrow sphere-in-perforated lamellae (SphPL) as a function of diblock copolymer volume fraction ϕ_{AB} at $\chi_{AB}N=\chi_{BC}N=23$ and $\chi_{AC}=1.75\chi_{AB}$.

grand canonical ensemble SCFT calculations. The resulting phase diagrams reveal unprecedented morphological richness, including 15 ordered phases. We believe this represents the proverbial tip of the iceberg, exposing nearly unlimited possibilities made possible by mixing two simple linear block polymers.

MODEL AND METHOD

Our work focuses on the self-assembly of incompressible binary blends composed of an AB diblock copolymer (Figure 1a) and an ABC triblock terpolymer that is either asymmetric (Figure 1b) or symmetric (Figure 1c) in end-block compositions. All diblock and triblock polymers are modeled as infinitely flexible Gaussian chains with equal statistical segment length b and equal segment volume ν . The parameter space of this binary blend system is very expansive with eight independent parameters, so we restrict our investigation to the block compositions and relationship between the χ_{ii} values in Figure 1. Our SCFT calculations predict that for the wide range of χ_{AB} where the diblock forms the G phase in the neat states, GA is the most stable network phase for both compositionally asymmetric and symmetric ABC triblock terpolymers in their respective neat states (Figure 1). Owing to our interest in the potential of block polymers to form network phases, we hypothesized that these systems would be reasonable starting points to identify novel phase behavior in AB/ABC blends.

In SCFT, prediction of the equilibrium phases requires identifying competing candidate phases based on empirical experience, ³⁸ so it is important to consider a reasonable set of candidate phases. In the Supporting Information Section S1.4, we list the 24 ordered structures considered in this study and explain why those candidates are chosen. The candidates include well-known equilibrium and metastable structures experimentally observed and theoretically predicted in AB diblock or ABC triblock polymer melts. ^{1,10,18,19} Here, we explain only the stable phases observed in our SCFT calculations and defer the explanations of the metastable phases to the Supporting Information Section S1.4.

For the network phases, double gyroid (G) is stable as the bicontinuous network in AB-rich blends, whereas alternating gyroid (GA) and core-shell networks with C cores, i.e., coreshell gyroid (CSG) and core-shell Fddd (CSO⁷⁰), are stable as the tricontinuous network phases (see Figure 2). As hybrid network morphologies, we observe cylinder-in-O⁷⁰ (CylO⁷⁰), where cylinder-like C tubular domains are hexagonally arranged at interstitial positions between A network nodes (Figures 2 and S11). For cylindrical phases, hexagonal-packed cylinders (C₆) is stable for the AB-rich blends, and hexagonalpacked alternating cylinders (C_{6a}^{A}), with A majority cylinders (Figure 2) and square-packed alternating cylinders (C₄^A), are stable as three-microdomain cylindrical phases. For lamellar phases, we consider conventional lamellae (L) with periodic AB layers for the AB-rich blends and alternating lamellae (LA) with ABCBA layers for the three-microdomain lamellar phase. For spherical phases, conventional body-centered cubic packing (BCC) is considered for the AB-rich blends. As binary alternating spheres, CsCl-type spheres (CsCl, Figure 1), NaCl-type spheres (NaCl, Figure 1), and Li₃Bi-type spheres (Li₃Bi) where the binary spherical crystalline structures having asymmetric coordination numbers are included.³⁹ As a hybrid spherical phase, we also observe a stable spheres-in-perforated lamellae (SphPL) phase (Figure 2), where spherical C domains are interstitially positioned between the holes of A perforated lamellar domains. Besides the candidates we consider here, there are a nearly unlimited number of additional candidates one can consider, for example, hybrid sphere-cylinder structures.³⁶ However, because our focus in this study is on the blends of diblock and triblock typical for network phase

formation, where block compositions are not very asymmetric, we assume those extra hybrid structures would not be stable relative to the candidates we consider in this study.

To determine the stable phase structures, we calculate the free energies of each candidate phase using canonical ensemble SCFT. On the basis of the equilibrium structures found from the canonical ensemble calculations, we then construct the phase diagrams by identifying the blend compositions of the coexisting phases, using grand canonical ensemble SCFT, which is a powerful tool for understanding the phase behavior of multicomponent systems. The SCFT calculations are performed using the CPU version of the open-source C++ PSCF software, where the self-consistent mean-field solutions for both canonical and grand canonical ensembles are found by numerically solving the modified diffusion equations in SCFT. The details of SCFT formalism for the blend systems and simulation methods are provided in Section S1 of the Supporting Information.

RESULTS

Phase Behavior with an Asymmetric ABC Triblock.

Because we are interested in network phase formation, we consider first the result of blending G^A -forming asymmetric ABC triblock and G-forming AB diblock, which we would anticipate are one of the promising starting points for realizing novel network phase behavior. On the basis of the neat melt phase behavior provided in Figures 1a and 1b, we examine the binary asymmetric ABC/AB blend at $\chi_{AB}N=23$; a symmetric triblock example (Figure 1c) will be considered in the following subsection. Figure 3 shows the resulting free energy curves, including only those phases that have a stability window. Figure S1 provides the complete free energy plot including the results for all candidate phases.

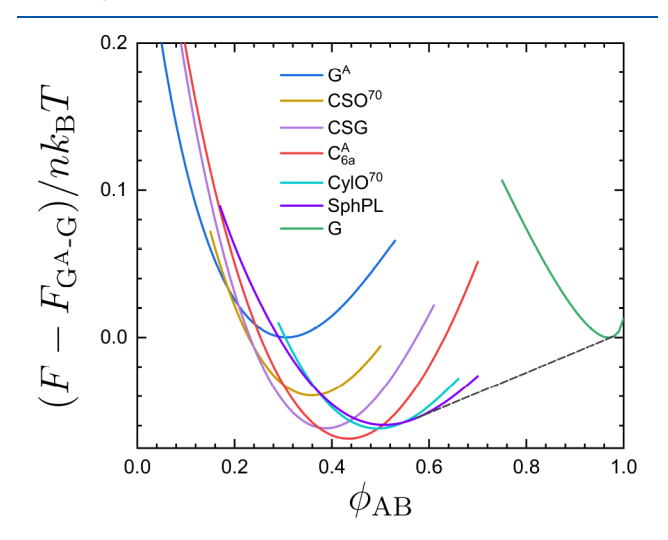


Figure 3. Relative free energy per chain of diblock size N for the stable phases with respect to the double tangent line between ABC-rich G^A and AB-rich G phases as a function of AB diblock volume fraction ϕ_{AB} in the binary blend of the asymmetric ABC triblock terpolymer and the AB diblock copolymer. The interaction parameters are $\chi_{AB}N=\chi_{BC}N=23$ and $\chi_{AC}=1.75\chi_{AB}$, and the overall length of the triblock is N'=2.32N. The block volume fractions for the triblock and diblock are $f_A'=0.2$, $f_B'=0.65$, $f_C'=0.15$, and $f_A=0.357$ (Figure 2). The dark gray dashed line is the common tangent between the SphPL and G phases, illustrating the wide two-phase macrophase-separated region when the diblock copolymer is the majority component.

Due to the large difference in size of the AB and ABC polymers, the free energy curves for F/nk_BT are tilted, as shown in Figure S2. For visualization purposes, Figure 3 presents the free energy values with respect to the double tangent line between the GA and G free energy curves. In this way, any free energy curve below the GA-G tangent line indicates that the associated microphase outcompetes the macrophase-separated states of GA and G. The detailed comparisons between the free energy curves for determining stable phases are presented in the additional relative free energy plots in Figure S4. In the canonical ensemble, the locations of coexisting phase compositions are usually found by double tangent construction on F/nk_BT curves for satisfying the equilibrium condition for equal chemical potentials. In fact, the double tangent construction method can be used on any relative free energy curves provided that the free energy values are subtracted by a linear function of ϕ_{AB} , which just provides a constant offset to the chemical potential that is independent of composition. For example, the common tangent lines between the SphPL and G phases in Figures S2 and S3 produce the same coexisting compositions ($\phi_{AB}^{SphPL} = 0.574$ and $\phi_{AB}^{G} =$ 0.978) as in Figure 3.

The free energy data reveal five stable ordered states between GA and G in the mixture, depending on the blend composition, with the phase sequence presented in Figure 2. While the triblock-rich phases are separated by narrow twophase regions, there is a wide two-phase coexistence window between the SphPL and G phases. Progressing from pure G^A to pure G, the CSO⁷⁰ phase first appears to be stable at relatively small volume fraction of the AB diblock, and the CSG is stable at higher compositions, as confirmed in the magnified free energy plot in Figure S4a. With the molecular parameter values we use here, the overall C block volume fraction $\overline{\rho}_{C}$ changes from 0.15 to 0 as ϕ_{AB} goes from 0 to 1, while the corresponding variation of overall B block volume fraction is very small (from $\bar{\rho}_{\rm B}$ = 0.65 to 0.64). The CSG structures comprise C core networks with very low overall volume fraction ($\bar{\rho}_{\rm C} \approx 0.1$) and very asymmetric core and shell volume compositions, which is unusual compared to those of traditional core-shell network structures reported in the literature. 18,22,34,42 However, the cubic unit cell size of CSG structure is about twice as large as than that of GA, which makes the C network volume per unit cell for CSG phase much larger than that for the G^A phase (Figure S15).

When the volume fractions of diblock and triblock are comparable, a C^A_{6a} structure appears as a stable phase, where both A and C blocks form cylindrical domains. Past the C^A_{6a} phase, the CylO70 phase becomes stable over a very narrow composition window ($\Delta\phi_{\rm AB}\approx 3\times 10^{-3}$), where chemical identities of the core network domain and matrix domain are now inverted by the reduced relative amount of C blocks. In this phase, the tubular C domains are interstitially positioned between the O⁷⁰ network composed of A blocks. For further information about the CylO70 morphology, we provide the segmental density distributions, isosurfaces of the tubular domains, and the unit cell dimensions in Figure S11. This hybrid phase has never been predicted in block copolymers. Increasing the diblock volume fraction further reduces the overall C block volume fraction, and SphPL appears as the final stable blended phase, with the spherical C domains interstitially located between the holes of perforated lamellar domains composed of A blocks. There is then a wide twophase region, occupying almost half of the range in ϕ_{AB} , until AB-rich G becomes the stable state.

Having examined in detail the behavior of this system at $\chi_{AB}N=23$, we proceed in Figure 4 to construct the phase

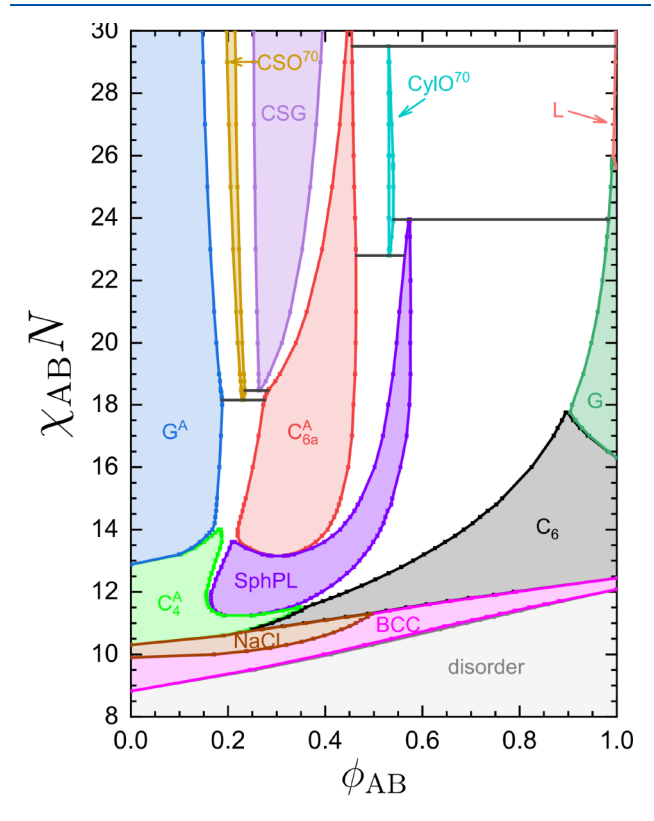


Figure 4. Phase diagram of the binary asymmetric ABC/AB blend where the degrees of polymerization are the same as in Figures 2 and 3. Here, N represents the total degree of polymerization of the diblock, and $\chi_{AB} = \chi_{BC}$ and $\chi_{AC} = 1.75\chi_{AB}$. The horizontal dark gray lines identify the invariant points where three phases are in equilibrium.

diagram for the asymmetric ABC/AB blend with respect to segregation strength and blend composition. As summarized in Figure 1, the stable phase sequence for the pure asymmetric ABC triblock terpolymer is BCC \rightarrow NaCl \rightarrow C₄^A \rightarrow G^A, and the stable phase sequence for the pure AB diblock copolymer is $BCC \rightarrow C_6 \rightarrow G \rightarrow L$ with increasing the segregation strength $\chi_{AB}N$ over the range studied here. For the BCC sphere phase formed in the pure ABC or ABC-rich blends, the bcc spheres are A domains and, for the triblock copolymer, the C segments are mixed in the B matrix domains (Figure S13). On the phase diagram, white empty regions correspond to the two-phase coexistence windows, and any state within the two-phase widows is associated by a horizontal (constant temperature) tie line connecting the boundary phases for a macrophaseseparated state. We also denote the invariant points with the horizontal tie lines where three phases are in equilibrium. A magnified portion of the phase diagram for the invariant points is provided in Figure S6.

As anticipated from the results at $\chi_{AB}N=23$, a wide two-phase coexistence window is located next to the AB-rich phase windows (L, G, and C₆) for most segregation strengths, while rich one-phase behavior is exhibited on the ABC-rich side. Remarkably, the stability window for C_{6a}^A spans a wide range of $\chi_{AB}N$, even up to the values where the diblocks form a lamellar

phase in the neat melt. On the left side of the C_{6a}^A window, the stability windows for the core—shell network phases, CSO^{70} and CSG, extend to high $\chi_{AB}N$ values, and it is interesting that the core—shell network phases remain stable even for a mixture of L-forming diblock and G^A -forming triblock. The hybrid phases, i.e., $CylO^{70}$ and SphPL on the right side of the C_{6a}^A window, tend to be destabilized with increasing $\chi_{AB}N$, leaving a wider two-phase window at higher $\chi_{AB}N$ values.

One notable feature of this phase diagram is that the CylO⁷⁰ stability window occupies an extremely narrow composition range at around $\phi_{AB} \approx 0.533$, resembling the feature of a phase field in a metal alloy phase diagram. ^{43–45} As the segregation strength increases, the phase field gets narrower and a eutectoid transformation takes place at around $\chi_{AB}N \approx 29.5$ with macrophase separation into C^A_{6a} and L phases. Another interesting feature is that a relatively wide SphPL stability window appears between the C₄^A and C₆ windows, which indicates that SphPL emerges in the mixture composed of C₄forming triblock and C₆-forming diblock. Here, mixing classical cylinder morphologies in the diblock and triblock leads to a nonclassical hybrid morphology combining geometries that are different from the parent ones. We also note that the C_{6a}^{A} phase window is located right above the SphPL phase window, which means that there is an intriguing cylinder \rightarrow SphPL \rightarrow cylinder transition, for example, when increasing $\chi_{AB}N$ at $\phi_{AB}=0.3$. The reemergence of the cylindrical morphology is understood by recognizing that the C_{6a} structure can be constructed from SphPL by fusing the C spheres into C columns and the bulky PL junctions into A columns.

Phase Behavior with a Symmetric ABC Triblock. We now examine the phase behavior in an AB/ABC blend with a triblock that is symmetric in block composition (Figure 1c). Following the same approach used for the asymmetric case, we thus begin by examining the phase behavior at $\chi_{AB}N=23$ with $\chi_{AB}=\chi_{BC}$ and $\chi_{AC}=1.75$ χ_{AB} . In the blend of symmetric G^A-forming triblock and G-forming diblock at $\chi_{AB}N=23$ (Figure 5), the CSO⁷⁰, CSG, and C^A_{6a} phases are stable in the same order as in the asymmetric ABC/AB blend, but the CylO⁷⁰ and SphPL hybrid phases are not observed in this symmetric system. Examining the phase behavior at $\chi_{AB}N=23$ in more

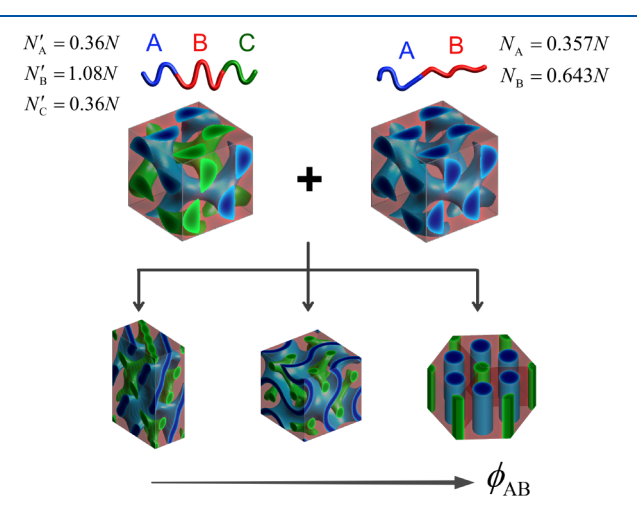


Figure 5. Schematic illustrating morphologies associated with blending the G^A -forming symmetric ABC triblock terpolymer and the G-forming AB diblock copolymer, which results in the phase sequence $CSO^{70} \rightarrow CSG \rightarrow C_{6a}^A$ as a function of diblock copolymer volume fraction ϕ_{AB} at $\chi_{AB}N = \chi_{BC}N = 23$ and $\chi_{AC} = 1.75\chi_{AB}$.

detail, the corresponding free energy plot in Figure 6 reveals a wide two-phase coexistence window between the C_{6a}^{A} and G

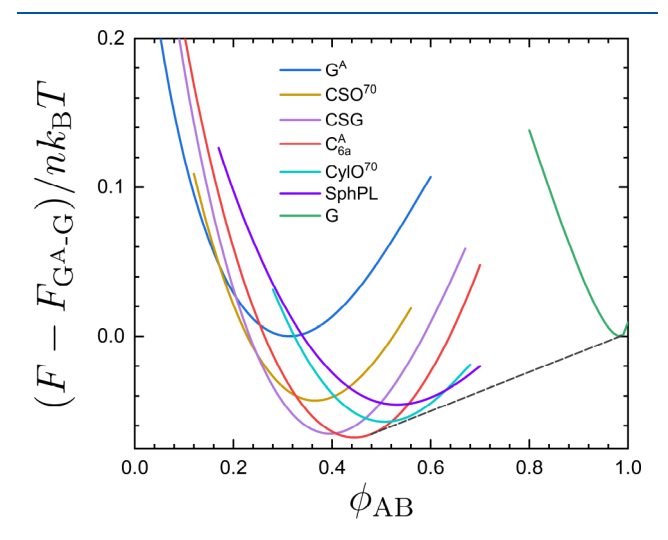


Figure 6. Relative free energy per chain of diblock size N for the stable phases with respect to the double tangent line between G^A and G phases as a function of AB diblock volume fraction ϕ_{AB} in the binary blend of the symmetric ABC triblock terpolymer and the AB diblock copolymer at $\chi_{AB}N = \chi_{BC}N = 23$ and $\chi_{AC} = 1.75\chi_{AB}$, where the overall length of triblock is N' = 1.8N. The block volume fractions for the triblock and diblock are $f'_A = 0.2$, $f'_B = 0.6$, $f'_C = 0.2$, and $f_A = 0.357$ (Figure 5). The dark gray dashed line is the common tangent line between the C^A_{6a} and G phases representing macrophase separation into the two phases. Data for all of the candidate phases are included in Figure S7.

curves, indicated by the tie line. The free energy curves for CylO^{70} and SphPL phases are located above the tie line, which means that the macrophase separation into C_{6a}^{A} and G phases now outcompetes the microphase separation into the hybrid phases.

Figure 7 shows the phase diagram constructed for the binary blend with the symmetric ABC polymer. Compared to the asymmetric case, the CylO⁷⁰ and SphPL stability windows are absent on the right side of the $C_{6a}^{\mbox{\scriptsize A}}$ stability window. A wide two-phase coexistence window is located again proximate to the AB-rich phases, similar to the asymmetric phase diagram (Figure 4). Aside from the absence of CylO⁷⁰ and SphPL windows, the topology of the upper part of the phase diagram is almost the same as the previous one in Figure 4, but the lower part is complicated and different. For clarity, magnified portions of the phase diagram for the lower part and for invariant points are provided in Figures S8 and S10, respectively. The SphPL stability region is diminished by the emergence of an Li₃Bi phase window. The Li₃Bi structure, which has unequal coordination numbers for A and C spheres, has never been observed in pure symmetric ABC triblock terpolymers, but it has been predicted by SCFT calculations in ABCB terpolymer melts with equal volume fraction of A and C blocks.39

As the different polymer blocks become strongly incompatible at high segregation strength, the diblock and triblock become increasingly immiscible, and the termination of the C_{6a}^{A} phase region results in a wider two-phase coexistence region between the CSG and L phases than the region for the blend with the asymmetric triblock terpolymer. However, both CSO⁷⁰ and CSG phase regions continue with almost vertical

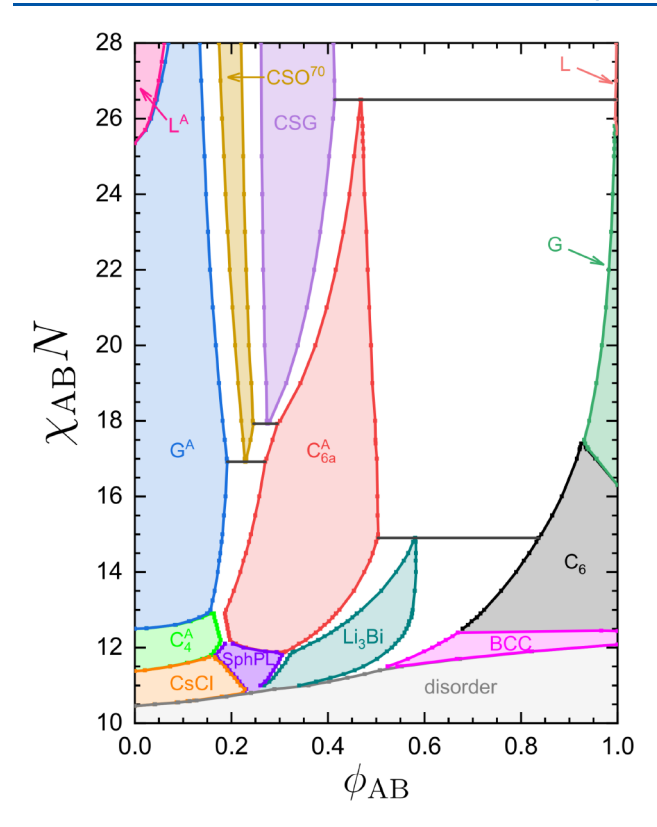


Figure 7. Phase diagram of the binary symmetric ABC/AB blends where the degrees of polymerization are the same as in Figures 5 and 6. Here, N represents the total degree of polymerization of the diblock, and $\chi_{AB} = \chi_{BC}$ and $\chi_{AC} = 1.75\chi_{AB}$. The horizontal dark gray lines identify the invariant points where three phases are in equilibrium. Free energy data for computing the particle-forming region of the phase diagram are provided in Figure S9.

phase boundaries to the high $\chi_{AB}N$ values where the diblock copolymer self-assembles into an L phase in the neat melt. The vertical phase boundaries imply that the relative stabilities of the microphases become less dependent on segregation strength with increasing $\chi_{AB}N$.

DISCUSSION

Two-Phase Coexistence Window. The existence of a wide two-phase coexistence window next to the AB-rich phases is a generic feature of the AB/ABC blend system and illustrates the impact of the relative miscibility of the two components. This phase behavior can be explained by the entropy and enthalpy for mixing of polymers. When AB diblock and ABC triblock polymers are mixed, the system gains entropy of mixing but suffers an enthalpic penalty caused by unfavorable interactions between the C blocks and the other blocks. In ABC-rich mixtures, the unfavorable contact energy can be minimized by orienting the AB diblocks parallel to the direction of ABC triblocks in the same microdomains, so it is relatively easier to mix a small amount of AB diblock into ABC triblock microdomains than vice versa. The driving force for mixing can be quantified by the relative free energy values with respect to pure GA and G states, as shown in Figure S3 for the asymmetric ABC/AB blend. Upon mixing with the diblocks, the entropic gain prevails over the enthalpic penalty, favoring mixed states until a considerable amount of the diblock is added.

For the AB-rich mixtures with small amounts of triblock, the C segments mix within the B domains formed by the diblocks. This behavior is simplest to understand for the lamellar morphology, as shown in Figure 8a. With higher triblock

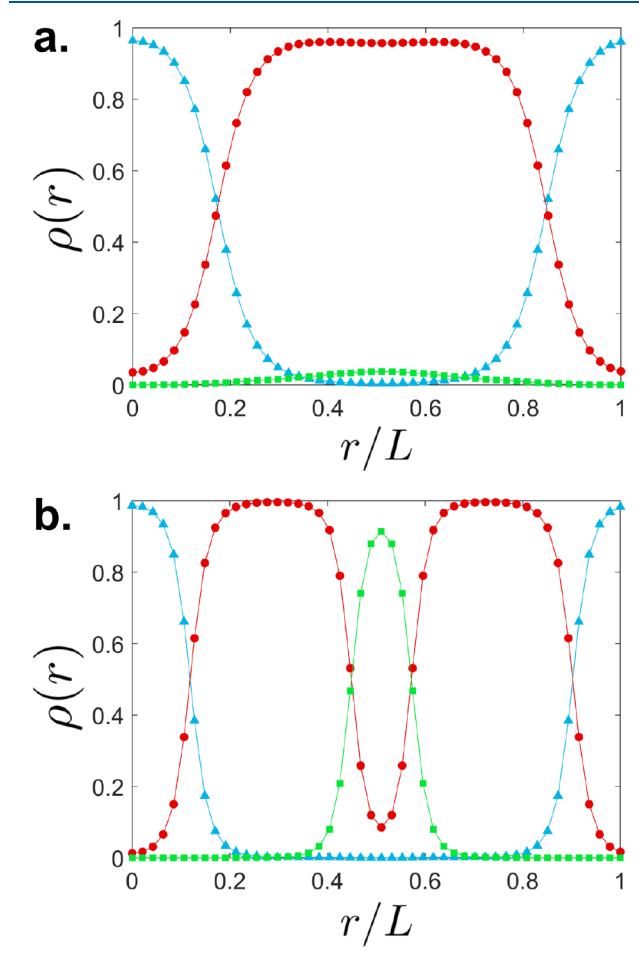


Figure 8. Segmental density variations within the lamellar phases at (a) $\phi_{AB} = 0.9$ and (b) 0.2 for the binary asymmetric ABC/AB blend corresponding to Figure 3. The blue triangles, red circles, and green squares correspond to the segmental density distributions for A, B, and C blocks $(\rho_A(r), \rho_B(r), \text{ and } \rho_C(r))$, respectively. The driving forces for mixing into the L and L^A phases are shown in Figure S3, and the supplemental results at other ϕ_{AB} values are provided in Figure S12.

composition, the increasing enthalpic penalty of unfavorable B/C interactions reduces the driving force for mixing until the lowest free energy state can be achieved by forming separate C domains, which minimizes unfavorable B/C contacts (Figure 8b). This general morphological trend is observed for other ordered states as well, but they are harder to visualize because the segmental density profiles are not one-dimensional. For example, when maintaining the symmetry of the neat state AB structures, the free energies of the resulting AB-rich phases, e.g., L, G, and C₆ in Figure S3, increase with increasing triblock volume fraction due to the unfavorable B/C contact energy, with an exception for the almost pure mixtures ($\phi_{AB} \approx 1$), which are stabilized by a large entropy of mixing. The key difference occurs for the SphPL and CylO70 states. Compared to the AB-rich phases, the mixing into SphPL and CylO⁷⁰ phases are thermodynamically favorable due to the interstitially segregated C domains, which minimize the B/C contacts. As a

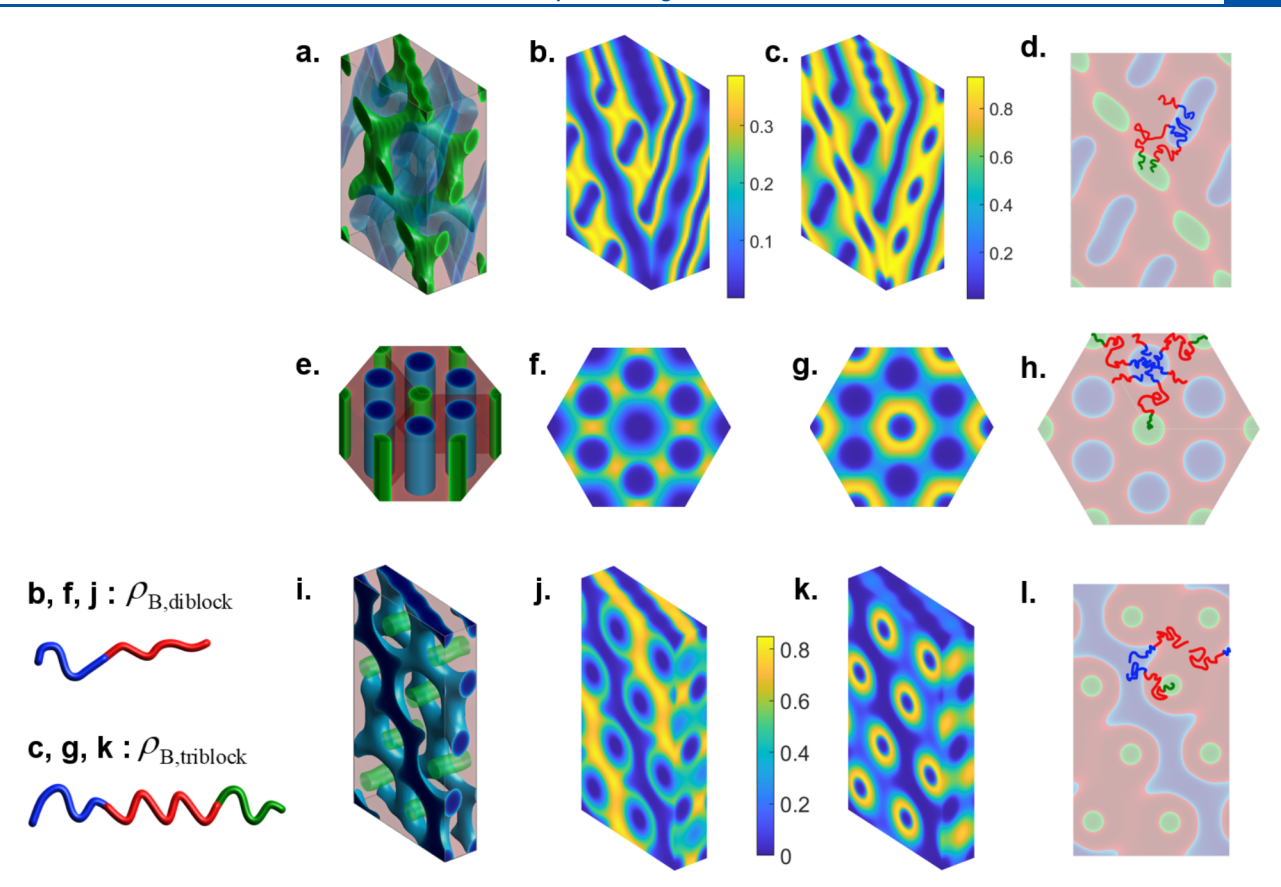


Figure 9. Morphologies, segmental density distributions, and schematics of chain conformations for CSO⁷⁰ at $\phi_{AB} = 0.22$ in the first row (a, b, c, d), C_{6a}^{A} at $\phi_{AB} = 0.45$ in the second row (e, f, g, h), and CylO⁷⁰ at $\phi_{AB} = 0.533$ in the third row (i, j, k, l), observed as equilibrium phases in Figure 3. The first column (a, e, i) shows the morphologies with the core structures highlighted. The second column (b, f, j) shows the spatial distributions of the B segment of the diblock. The third column (c, g, k) shows the spatial distributions of the B segment of the triblock. The last column (d, h, i) schematically illustrates chain conformations in each phase. The color bar in the middle of the bottom row is associated with the distributions in (f, g, j, and k).

result, these morphologies appear as equilibrium phases next to the wide two-phase window on the AB-rich side of the phase diagram (Figure 4).

Binary Self-Assembled Morphologies. We now discuss in detail the morphologies of the stable phases observed in the Results section. The mechanism to form SphPL by blending C_4^A and C_6 in the asymmetric ABC/AB blend (Figure 4) can be understood by the same argument used by Goldacker et al.³⁴ to rationalize the formation of CSG in their binary blend of symmetric L^A-forming ABC triblock and symmetric L-forming AB diblock. In the pure C₄^A phase, the same numbers of AB and BC junction points are homogeneously distributed along the A/B and B/C interfaces, respectively. However, when diblocks are added, the A and B domains of C₄^A are swelled by AB diblocks, and the number of A/B junction points on the interface increases while the number of B/C junction points remains constant. In order to minimize the conformational entropy loss associated with chain stretching by the crowded interface, spontaneous curvature toward the C domain occurs, allowing A and B blocks to relax by distributing their junctions on the wider interface of PL, which have cylinder-like connectors but lower average mean curvature, at the cost of stretching the C blocks to form spherical domains.

For the core—shell network morphologies CSO⁷⁰ and CSG, the overall volume fractions of the C core networks are very low relative to the associated B shell domain volume fractions. This behavior in the AB/ABC blend differs from what has been

observed in other systems. Explicitly, CSO⁷⁰ and CSG network phases were first observed in neat compositionally asymmetric ABC triblock terpolymers. 11,16,31 Recently, the CSG phase was predicted in neat melts of a topologically asymmetric A(BC)_m miktoarm star copolymer with A core network.⁴⁶ In these other cases, spontaneous curvature towards the core domain occurs due to the tendency to maximize the conformational entropy of asymmetric polymers. Compared to those neat triblock terpolymers, the block compositions of the triblocks we used are relatively symmetric ($f_A = 0.2, f_B' = 0.65, f_C' = 0.15,$ and $f'_A = 0.2$, $f'_B = 0.6$, $f'_C = 0.2$), whereupon the spontaneous curvature toward C blocks occurs to reduce chain stretching energy in A and B domains swelled by the AB diblocks. Our explanation is reminiscent of that used to explain the observation of CSG formation from LA-forming ABC triblocks34 and CSG-forming ABC triblocks22 with an inverted core network, where addition of AB diblocks induced changes in interfacial curvatures. We will provide shortly a self-assembly mechanism that accounts for the unusually asymmetric volume fractions of core and shell domains with the molecular distributions in CSO⁷⁰ morphology.

To understand the self-assembly mechanism for the morphologies observed in CSO⁷⁰, C_{6a}^{A} , and CylO⁷⁰ phases, Figure 9 shows the spatial distributions of B blocks for the binary asymmetric ABC/AB blends of Figure 3. In these blends, the B block of the triblock is much longer ($N_{B}' = 1.5N$) than the B block of the diblock ($N_{B} = 0.643N$), and they are

preferentially localized in the B domains of each morphology. The effect of block length dispersity on interfacial curvature has been well demonstrated by prior studies on self-assembly of block copolymer blends, 21,24,30,47,48 where blocks of different length are preferentially distributed within the same domain to reduce the chain stretching penalty associated with filling the center of the domain where high packing frustration is believed to exist. This heterogeneous distribution of blocks leads to localization of different block junctions along the interface, which reduces the cost for deviating from constant mean curvature and produces unusual structures, which are thermodynamically unfavorable in neat block copolymer melts.

For the CSO⁷⁰ phase in Figure 9, the B blocks of the diblocks are distributed close to the A matrix domain (Figure 9b) while the B blocks of the triblocks surround the C network domain as a shell structure (Figure 9c). The diblocks filling the space far away from the C core network relieve the packing frustration in the B domain for the triblocks, forming a network structure with very asymmetric volume fractions of core and shell domains. We note that the diblocks are distributed along the flat interfaces of the A domain, and this result supports our observation that the stability of the CSO⁷⁰ phase exists in the blends consisting of L-forming diblocks.

In the C_{6a}^A phase, both the A and C blocks form cylindrical domains in a matrix of B blocks. The spatial distributions of the B blocks show that the B blocks of the triblock surround the C cylinders (Figure 9g), and the B blocks of the diblock fill the space in the B domain far from the C cylinders (Figure 9f), which relieves the stretching penalty of the middle blocks in the triblock that are bridging the A and C cylinders. An interesting feature of the phase diagrams in Figures 4 and 7 is that even when the diblock and triblock are not cylinderforming in the neat melt states (e.g., G^A , G, and L), their binary blends self-assemble into the C_{6a}^A phase at certain blend compositions over a wide range of $\chi_{AB}N$. This robust stability of C_{6a}^A can be explained by the core—shell distribution of A blocks shown in Figure 10. Here, the shorter A blocks of the diblock form the shell structure while the longer A blocks of

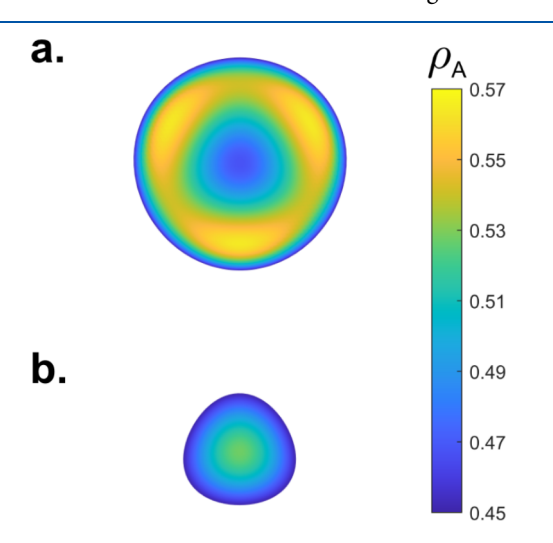


Figure 10. Segmental density distributions within the isosurfaces $\rho_{\rm A}({\bf r})=0.45$ of one of the A cylinders for the equilibrium ${\rm C}_{6a}^{\rm A}$ in Figure 9. (a) Spatial distribution of A segments of the diblock. (b) Spatial distribution of A segments of the triblock. The locations of all 6-fold A cylinders in the hexagonal unit cell for the ${\rm C}_{6a}^{\rm A}$ phase are presented in Figure S14.

the triblock form the core structure along the radial direction within the A cylindrical domains, which prevents the shorter A blocks from excessively stretching to fill the center of the cylindrical domains. We speculate that along with the localization of B blocks the core—shell distribution of A blocks reduces the total entropic cost of forming the C_{6a}^{A} phase, which adopts constant mean curvature A and C domains to minimize interfacial energy at high segregation strength.

The bottom row of Figure 9 shows the corresponding results for the CylO^{70} morphology. The long B blocks of the triblock extend to fill the space, which are far away from the nodal regions of the O^{70} network, and surround the C tubular domains. We posit that the local segregation of bidisperse B blocks in the B domain facilitates stabilizing the unusual CylO^{70} morphology, which does not exist in the respective pure melts.

Effect of Triblock Asymmetry. In this study, we considered the specific block compositions of the triblocks and diblocks in Figure 1 and examined the phase behaviors of their blends. Because of an expansive parameter space for binary AB/ABC blend systems, it is computationally challenging to construct all the possible phase diagrams. From the previous discussions, we infer that C block volume fraction has a critical impact on the relative miscibility of AB diblock and ABC triblock and on formation of the self-assembled morphologies. In order to extend our understanding of the phase behaviors, we further investigate the effect of C block length variation on the stability of the phases we observed in the asymmetric ABC/AB blend in Figure 3. Figure 11 presents the resulting phase diagram with respect to length

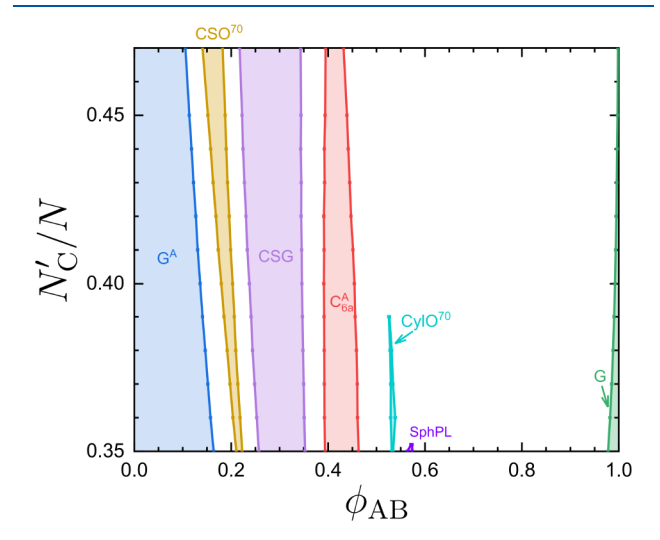


Figure 11. Phase diagram with respect to the ratio of the C block length $N_{\rm C}'$ to the AB diblock length N and blend composition of diblock $\phi_{\rm AB}$ for the asymmetric ABC/AB blend at $\chi_{\rm AB}N=\chi_{\rm BC}N=23$ and $\chi_{\rm AC}=1.75\chi_{\rm AB}$. The A and B block lengths are fixed at $N_{\rm A}'=0.47N$ and $N_{\rm B}'=1.5N$ for the triblock and $N_{\rm A}=0.357N$ and $N_{\rm B}=0.643N$ for the diblock.

ratio of the C block to diblock for the fixed interaction parameters and other block lengths. In the considered range of $N_{\rm C}/N$, the triblock ranges from asymmetric to symmetric block compositions, forming ${\rm G^A}$, while the G-forming diblock block composition remains the same. Between the ${\rm G^A}$ and G phase regions, the CSO⁷⁰ and CSG remain stable over the range examined here, but the CylO⁷⁰ and SphPL are destabilized as

the ABC triblock architecture becomes more symmetric. The reduced difference between $f'_{\rm B}$ and $f'_{\rm C}$ by increasing the C tail block length can account for the destabilization of those hybrid phases by disfavoring the spherical or cylindrical C domain formation. The increased degree of symmetry of the triblock architecture can also be a factor destabilizing the asymmetric hybrid morphologies, as molecular asymmetry promotes formation of hybrid geometry nanostructures. 46 The narrowed G stability region with increasing $N'_{\rm C}/N$ indicates decreased miscibility between the two components due to the increased amount of incompatible C blocks for the AB diblocks. Aside from the destabilization of hybrid phases, the stable phase sequence in the systems considered in Figure 11 remains the same as that observed in Figures 3 and 6. We note in particular that CSO⁷⁰ and CSG phases remain stable with considerable variation of the C block length. In fact, the network volume fraction is relatively robust to the variations of the C block length. For example, at ϕ_{AB} = 0.3, the overall C block volume fraction of CSG changes from $\overline{\rho}_{\rm C}$ = 0.11 to 0.13 in the range of $N'_{\rm C}/N$ we considered here, which implies that the relative size of the network channel is not very sensitive to theC block length relative to the diblock length.

We expect that in the very strong segregation limit, where both the diblock and the triblock are highly stretched and form lamellae with very narrow interfaces in their respective neat states, all intermediate phases such as CSO^{70} , CSG, and C_{6a}^{A} in both phase diagrams (Figures 4 and 7) would be destabilized, leaving a wide two-phase coexistence region between almost pure L^A and L phases. In other words, macrophase separation into nearly pure LA and L phases would prevail over other intermediate phases in mixed states. Furthermore, it might be possible to mix individual lamellar structures on a supermolecular level with the centrosymmetric sequence (...ABC CBA AB BA ABC...) in the strong segregation limit. According to a theoretical study on blends of ABC and AB block copolymers based on the strong segregation assumption,³² a lamellar structure mixed on the molecular level with the same A and B domains is stable under the condition that the interfacial tension of the diblock copolymer $\gamma_{AB} \sim \chi_{AB}^{-1/2}$ is larger than the interfacial tension within the triblock terpolymer $\gamma_{\rm BC} \sim \chi_{\rm BC}^{1/2}$, which is not the case in our study, where $\chi_{AB} = \chi_{BC}$.

Considering the expansive parameter space for a binary AB/ ABC blend system, another region worth exploring in detail is where the A block lengths of the two polymers differ significantly. Previous literature suggests that the double diamond phase, which is metastable in neat AB diblock copolymers, can be stabilized using block copolymer blends or block copolymer/homopolymer blends because the local segregations of network-forming blocks with large length differences relieves the packing frustration at the four-branched nodes of the diamond phase. ^{24,30,49} Because the relative length ratio values of the A blocks we used in this study are not significantly high $(N'_A/N_A = 1.32 \text{ or } 1.01)$, it would be interesting to explore whether the core-shell diamond or alternating diamond can be realized by strategically designing AB/ABC blend with highly disperse block lengths. There are many other possible directions for this research, including blends of non-network-forming AB diblock and ABC triblock.³⁶ In this context, additional phases, such as single gyroid, single diamond, plumber's nightmare, and abc stacking of perforated lamellar phases, might be considered as candidate structures.

CONCLUSION

In this article, we investigated the phase behavior of binary blends of AB diblock and ABC triblock polymers, where the triblock terpolymer is either symmetric or asymmetric in block composition, by identifying the stable phase structures and constructing the phase diagrams as a function of the segregation strength and the blend composition. Our SCFT calculations reveal that blending simple linear block polymers generates complex phase behaviors exhibiting a rich complement of phases, including hybrid morphologies and non-classical network morphologies, which are difficult or impossible to realize with neat block polymer melts. The diverse morphologies in the AB/ABC blends are promoted by the binary self-assembly through the preferential distributions of the same type blocks belonging to the different components in the same domains.

The limitation of SCFT prediction is that one should determine competing candidate phases before structural prediction, and there is a possibility that we did not thoroughly consider possible binary crystalline spherical structures for the low segregation regimes of the phase diagrams. However, due to the mean field assumption, the mean field theory predictions are mostly inaccurate near the order—disorder transition temperatures where composition fluctuations are strong, and our emphasis in this study is not on that part of phase diagram but on the network-phase-forming blends. If one were instead interested in focusing on sphere-forming binary AB/ABC blends, one could consider many different crystalline structures reported in the prior SCFT studies.^{39,44}

The emergence of a rich set of ordered-state structures with the specific block compositions in our study suggests that binary AB/ABC blend systems have the potential to produce nearly unlimited morphological richness with an expansive parameter space. In terms of simplicity and morphological richness, blending AB diblock copolymer and ABC triblock terpolymer provides a novel route to creating new network morphologies instead of precisely tuning complex molecular architecture in neat melts, 46 and thus provides significant advantages in designing advanced network nanomaterials for next-generation nanotechnology such as photonic crystals, solar cells, and membranes. 3–8

ASSOCIATED CONTENT

Supporting Information

The Supporting Information is available free of charge at https://pubs.acs.org/doi/10.1021/acs.macromol.2c02216.

Canonical and grand canonical SCFT formalism; simulation details; list of candidate phases; additional free energy results; additional grand canonical calculation results; magnified portion of the phase diagrams; morphologies of the CylO⁷⁰, L, L^A, BCC, and C^A_{6a} phases (PDF)

AUTHOR INFORMATION

Corresponding Authors

Kevin D. Dorfman — Department of Chemical Engineering and Materials Science, University of Minnesota—Twin Cities, Minneapolis, Minnesota 55455, United States; oorcid.org/0000-0003-0065-5157; Email: dorfman@umn.edu

Frank S. Bates – Department of Chemical Engineering and Materials Science, University of Minnesota—Twin Cities,

Minneapolis, Minnesota 55455, United States; oorcid.org/0000-0003-3977-1278; Email: bates001@umn.edu

Author

So Jung Park — Department of Chemical Engineering and Materials Science, University of Minnesota—Twin Cities, Minneapolis, Minnesota 55455, United States; orcid.org/0000-0002-3003-6501

Complete contact information is available at: https://pubs.acs.org/10.1021/acs.macromol.2c02216

Notes

The authors declare no competing financial interest.

ACKNOWLEDGMENTS

This work was supported primarily by the National Science Foundation through the University of Minnesota MRSEC under Award DMR-2011401. The Minnesota Supercomputing Institute (MSI) at the University of Minnesota provided computational resources that contributed to the research results reported in this paper.

REFERENCES

- (1) Bates, C. M.; Bates, F. S. 50th Anniversary Perspective: Block Polymers—Pure Potential. *Macromolecules* **2017**, *50*, 3–22.
- (2) Bates, F. S.; Fredrickson, G. H. Block Copolymers-Designer Soft Materials. *Phys. Today* **1999**, *52*, 32–38.
- (3) Crossland, E. J.; Kamperman, M.; Nedelcu, M.; Ducati, C.; Wiesner, U.; Smilgies, D. M.; Toombes, G. E.; Hillmyer, M. A.; Ludwigs, S.; Steiner, U.; Snaith, H. J. A bicontinuous double gyroid hybrid solar cell. *Nano Lett.* **2009**, *9*, 2807–2812.
- (4) Docampo, P.; Stefik, M.; Guldin, S.; Gunning, R.; Yufa, N. A.; Cai, N.; Wang, P.; Steiner, U.; Wiesner, U.; Snaith, H. J. Triblock-terpolymer-directed self-assembly of mesoporous TiO 2: High-performance photoanodes for solid-state dye-sensitized solar cells. *Adv. Energy Mater.* **2012**, *2*, 676–682.
- (5) Urbas, A. M.; Maldovan, M.; DeRege, P.; Thomas, E. L. Bicontinuous cubic block copolymer photonic crystals. *Adv. Mater.* **2002**, *14*, 1850–1853.
- (6) Stefik, M.; Guldin, S.; Vignolini, S.; Wiesner, U.; Steiner, U. Block copolymer self-assembly for nanophotonics. *Chem. Soc. Rev.* **2015**, *44*, 5076–5091.
- (7) Gin, D. L.; Bara, J. E.; Noble, R. D.; Elliott, B. J. Polymerized lyotropic liquid crystal assemblies for membrane applications. *Macromol. Rapid Commun.* **2008**, *29*, 367–389.
- (8) Li, L.; Schulte, L.; Clausen, L. D.; Hansen, K. M.; Jonsson, G. E.; Ndoni, S. Gyroid nanoporous membranes with tunable permeability. *ACS Nano* **2011**, *5*, 7754–7766.
- (9) Hajduk, D. A.; Harper, P. E.; Gruner, S. M.; Honeker, C. C.; Kim, G.; Thomas, E. L.; Fetters, L. J. The Gyroid: A New Equilibrium Morphology in Weakly Segregated Diblock Copolymers. *Macromolecules* **1994**, *27*, 4063–4075.
- (10) Matsen, M. W.; Bates, F. S. Origins of Complex Self-Assembly in Block Copolymers. *Macromolecules* **1996**, *29*, 7641–7644.
- (11) Tyler, C. A.; Morse, D. C. Orthorhombic *Fddd* Network in Triblock and Diblock Copolymer Melts. *Phys. Rev. Lett.* **2005**, *94*, 208302.
- (12) Bates, F. S. Network phases in block copolymer melts. MRS Bull. 2005, 30, 525-532.
- (13) Takenaka, M.; Wakada, T.; Akasaka, S.; Nishitsuji, S.; Saijo, K.; Shimizu, H.; Kim, M. I.; Hasegawa, H. Orthorhombic Fddd network in diblock copolymer melts. *Macromolecules* **2007**, *40*, 4399–4402.
- (14) Meuler, A. J.; Hillmyer, M. A.; Bates, F. S. Ordered network mesostructures in block polymer materials. *Macromolecules* **2009**, *42*, 7221–7250.

- (15) Wang, X. B.; Lo, T. Y.; Hsueh, H. Y.; Ho, R. M. Double and single network phases in polystyrene-block-poly(L-lactide) diblock copolymers. *Macromolecules* **2013**, *46*, 2997–3004.
- (16) Shefelbine, T. A.; Vigild, M. E.; Matsen, M. W.; Hajduk, D. A.; Hillmyer, M. A.; Cussler, E. L.; Bates, F. S. Core-shell gyroid morphology in a poly(isoprene-block-styrene-block-dimethylsiloxane) triblock copolymer. *J. Am. Chem. Soc.* **1999**, *121*, 8457–8465.
- (17) Epps, T. H.; Cochran, E. W.; Hardy, C. M.; Bailey, T. S.; Waletzko, R. S.; Bates, F. S. Network phases in ABC triblock copolymers. *Macromolecules* **2004**, *37*, 7085–7088.
- (18) Epps, T. H.; Cochran, E. W.; Bailey, T. S.; Waletzko, R. S.; Hardy, C. M.; Bates, F. S. Ordered Network Phases in Linear Poly(isoprene-b-styrene-b-ethylene oxide) Triblock Copolymers. *Macromolecules* **2004**, *37*, 8325–8341.
- (19) Qin, J.; Bates, F. S.; Morse, D. C. Phase Behavior of Nonfrustrated ABC Triblock Copolymers: Weak and Intermediate Segregation. *Macromolecules* **2010**, 43, 5128–5136.
- (20) Dorfman, K. D. Frank-Kasper Phases in Block Polymers. *Macromolecules* **2021**, *54*, 10251–10270.
- (21) Matsushita, Y.; Takano, A.; Vayer, M.; Sinturel, C. Nonclassical Block Copolymer Self-Assembly Resulting from a Constrained Location of Chains and Junctions. *Adv. Mater. Interfaces* **2020**, 7, 1902007.
- (22) Abetz, V.; Goldacker, T. Formation of superlattices via blending of block copolymers. *Macromol. Rapid Commun.* **2000**, *21*, 16–34.
- (23) Choi, C.; Ahn, S.; Kim, J. K. Diverse Morphologies of Block Copolymers by Blending with Homo (and Co) Polymers. *Macromolecules* **2020**, *53*, 4577–4580.
- (24) Takagi, W.; Suzuki, J.; Aoyama, Y.; Mihira, T.; Takano, A.; Matsushita, Y. Bicontinuous Double-Diamond Structures Formed in Ternary Blends of AB Diblock Copolymers with Block Chains of Different Lengths. *Macromolecules* **2019**, *52*, 6633–6640.
- (25) Hashimoto, T.; Yamasaki, K.; Koizumi, S.; Hasegawa, H. Ordered Structure in Blends of Block Copolymers. 1. Miscibility Criterion for Lamellar Block Copolymers. *Macromolecules* **1993**, 26, 2895–2904.
- (26) Hashimoto, T.; Koizumi, S.; Hasegawa, H. Ordered Structure in Blends of Block Copolymers. 2. Self-Assembly for Immiscible Lamella-Forming Copolymers. *Macromolecules* 1994, 27, 1562–1570.
- (27) Koizumi, S.; Hasegawa, H.; Hashimoto, T. Ordered Structure in Blends of Block Copolymers. 3. Self-Assembly in Blends of Sphereor Cylinder-Forming Copolymers. *Macromolecules* **1994**, 27, 4371–4381.
- (28) Yamaguchi, D.; Bodycomb, J.; Koizumi, S.; Hashimoto, T. Ordered structure in blends of block copolymers. 4. Location of the short diblock. *Macromolecules* **1999**, *32*, 5884–5894.
- (29) Yamaguchi, D.; Shiratake, S.; Hashimoto, T. Ordered structure in blends of block copolymers. 5. Blends of lamella-forming block copolymers showing both microphase separation involving unique morphological transitions and macrophase separation. *Macromolecules* **2000**, 33, 8258–8268.
- (30) Lai, C. T.; Shi, A.-C. Binary Blends of Diblock Copolymers: An Effective Route to Novel Bicontinuous Phases. *Macromol. Theory Simul.* **2021**, *30*, 2100019.
- (31) Bailey, T. S.; Hardy, C. M.; Epps, T. H.; Bates, F. S. A noncubic triply periodic network morphology in poly(isoprene-b-styrene-b-ethylene oxide) triblock copolymers. *Macromolecules* **2002**, *35*, 7007–7017.
- (32) Birshtein, T. M.; Zhulina, E. B.; Polotsky, A. A.; Abetz, V.; Stadler, R. Mixed supercrystalline structures in mixtures of ABC-triblock and AB(BC)-diblock copolymers, 1: Lamellar structures in bicomponent mixtures. *Macromol. Theory Simul.* **1999**, *8*, 151–160.
- (33) Birshtein, T. M.; Polotsky, A. A.; Abetz, V. Mixed supercrystalline structures in mixtures of ABC triblock and ab(bc) diblock copolymers, 3: Lamellar and cylindrical structures in bicomponent mixtures. *Macromol. Theory Simul.* **2001**, *10*, 700–718.
- (34) Goldacker, T.; Abetz, V. Core-Shell Cylinders and Core-Shell Gyroid Morphologies via Blending of Lamellar ABC Triblock and BC Diblock Copolymers. *Macromolecules* **1999**, 32, 5165–5167.

Macromolecules Article pubs.acs.org/Macromolecules

- (35) Jiang, S.; Göpfert, A.; Abetz, V. Novel Superlattices via Blending of Asymmetric Triblock Terpolymers with Diblock Copolymers. Macromol. Rapid Commun. 2003, 24, 932-937.
- (36) Ahn, S.; Kwak, J.; Choi, C.; Seo, Y.; Kim, J. K.; Lee, B. Gyroid Structures at Highly Asymmetric Volume Fractions by Blending of ABC Triblock Terpolymer and AB Diblock Copolymer. Macromolecules 2017, 50, 9008-9014.
- (37) Park, S. J.; Bates, F. S.; Dorfman, K. D. Alternating Gyroid in Block Polymer Blends. ACS Macro Lett. 2022, 11, 643-650.
- (38) Arora, A.; Qin, J.; Morse, D. C.; Delaney, K. T.; Fredrickson, G. H.; Bates, F. S.; Dorfman, K. D. Broadly Accessible Self-Consistent Field Theory for Block Polymer Materials Discovery. Macromolecules **2016**, 49, 4675–4690.
- (39) Xie, N.; Liu, M.; Deng, H.; Li, W.; Qiu, F.; Shi, A.-C. Macromolecular Metallurgy of Binary Mesocrystals via Designed Multiblock Terpolymers. J. Am. Chem. Soc. 2014, 136, 2974-2977.
- (40) Shi, A. C. Self-Consistent Field Theory of Inhomogeneous Polymeric Systems. In Var. Methods Mol. Model.; Wu, J., Ed.; Springer: Singapore, 2017; pp 155-180.
- (41) Matsen, M. W. Self-Consistent Field Theory and Its Applications. In Soft Matter; Gompper, G., Schick, M., Eds.; Wiley-VCH: 2007; Vol. 1: Polymer Melts and Mixtures, pp 87-178.
- (42) Tureau, M. S.; Kuan, W. F.; Rong, L.; Hsiao, B. S.; Epps, T. H. Inducing order from disordered copolymers: On demand generation of triblock morphologies including networks. Macromolecules 2012, 45, 4599-4605.
- (43) de Graef, M.; McHenry, M. E. Structure of Materials: An Introduction to Crystallography, Diffraction, and Symmetry; Cambridge University Press: Cambridge, 2012; Vol. 2.
- (44) Magruder, B. R.; Park, S. J.; Collanton, R. P.; Bates, F. S.; Dorfman, K. D. Laves Phase Field in a Diblock Copolymer Alloy. Macromolecules 2022, 55, 2991-2998.
- (45) Case, L. J.; Bates, F. S.; Dorfman, K. D. Tuning conformational asymmetry in particle-forming diblock copolymer alloys. Soft Matter, in press.
- (46) Dong, Q.; Li, W. Effect of Molecular Asymmetry on the Formation of Asymmetric Nanostructures in ABC-Type Block Copolymers. Macromolecules 2021, 54, 203-213.
- (47) Asai, Y.; Suzuki, J.; Aoyama, Y.; Nishioka, H.; Takano, A.; Matsushita, Y. Tricontinuous Double Diamond Network Structure from Binary Blends of ABC Triblock Terpolymers. Macromolecules 2017, 50, 5402-5411.
- (48) Asai, Y.; Yamada, K.; Yamada, M.; Takano, A.; Matsushita, Y. Formation of Tetragonally-Packed Rectangular Cylinders from ABC Block Terpolymer Blends. ACS Macro Lett. 2014, 3, 166-169.
- (49) Takagi, H.; Yamamoto, K.; Okamoto, S. Ordered-bicontinuousdouble-diamond structure in block copolymer/homopolymer blends. EPL 2015, 110, 48003.

□ Recommended by ACS

Structure and Phase Behavior of Bottlebrush Diblock **Copolymer-Linear Homopolymer Ternary Blends**

Bo Zhang, Frank S. Bates, et al.

FERRITARY 08 2023

MACROMOLECULES

READ 2

Effect of Changing Interfacial Tension on Fragmentation Kinetics of Block Copolymer Micelles

Supriva Gupta and Timothy P. Lodge

FEBRUARY 22, 2023

MACROMOLECULES

READ **C**

Chain Flexibility Effects on the Self-Assembly of Diblock **Copolymer in Thin Films**

Mingyang Chen, Xingkun Man, et al.

FEBRUARY 07, 2023

MACROMOLECULES

READ **C**

End-to-End Fluctuation of cis-Poly(isoprene) under Constraints from Slow Poly(*tert*-butyl styrene)

Zonghao Hong, Hongxia Guo, et al.

FEBRUARY 17, 2023

MACROMOLECULES

READ 2

Get More Suggestions >